Energy 262 (2023) 125464

Contents lists available at ScienceDirect

Energy

journal homepage: www.elsevier.com/locate/energy

Design optimization of a district heating and cooling system with a borehole seasonal thermal energy storage

Massimo Fiorentini [a,*], Philipp Heer [a], Luca Baldini [b]

[a] Urban Energy Systems Laboratory, Empa - Swiss Federal Laboratories for Materials Science and Technology, 8600 Dübendorf, Switzerland
[b] ZHAW Zurich University of Applied Sciences, 8401 Winterthur, Switzerland

ARTICLE INFO

Keywords:
Seasonal thermal energy storage
Energy optimization
Multi-energy systems
Renewable energy
CO_2 emissions reduction

ABSTRACT

The optimal design of borehole thermal energy storage systems can ensure their techno-economical goals are met. Current design optimization methods either employ detailed modelling unsuitable for numerical optimization or use simplified models that do not consider operational conditions. This paper proposes an optimization-oriented model and a non-convex optimization formulation that, differently from other studies in the literature, can consider the influence of the seasonal storage size and temperature on its capacity, losses, heat transfer rate, and efficiency of connected heat pumps or chillers. This methodology was applied to a case study, considering two scenarios: storing only the rejected heat from cooling and integrating solar thermal generation. Results show that, with varying boundary conditions such as the electricity CO_2 intensity profile, cooling demand, and price of carbon emissions, not only the optimal seasonal storage size changes but also its optimal operating conditions. The potential reduction of CO_2 emissions was found, under standard boundary conditions, to be limited (up to 6.7%), but an increase in cooling demand and an enhancement of the CO_2 intensity seasonal variation led to a reduction of 27.1%. Integration of solar generation further improved it to 43.7%, with a comparably small increase in annual cost, up to 6.1%.

1. Introduction

The carbon emission targets set for mid-century require the integration of energy technologies that are capable of supporting energy systems throughout the year. As reported by the International Energy Agency (IEA) [1], heat is the largest contributor to energy end-use, accounting for half of global final energy consumption, significantly more than electricity and transport, which account for 30% and 20% of the total demand respectively. In this report, renewable generation is estimated to have met only 11% of global heat demand in 2019. A temporal mismatch between the most common renewable heat generation, solar, and heat demand occurs on both a daily and a seasonal basis. Therefore, energy storage technologies play an important role in enabling the integration of a larger share of renewable generation in energy systems. While on a short time scale (e.g. hourly or daily) there are several energy storage technology options available to cover both thermal and electrical energy needs, on a seasonal scale there are fewer technologies readily available, and they are mostly thermal. As buildings' heating and cooling is one of the major sources of energy demand, integration of seasonal thermal energy storages (STESs) in energy systems can offer an attractive opportunity to shift solar heat generation from summer to winter and to capture waste heat from cooling or industrial operations.

Several seasonal thermal storage options are available, as presented in [2], and BTES systems are one of the most economical and effective solutions [3]. Historically, BTES systems were employed with centralized solar plants designed to operate at high temperature and supported district heating networks. The potential of BTES to improve the efficiency of district energy systems has been extensively investigated in simulation studies, as in [4], where the effectiveness of different BTES system configurations to support the heat delivery to a small-scale district integrating centralized solar generation was analysed, and in [5], where a parametric study was conducted on a similar system with centralized solar generation varying BTES and solar collector array sizes. Both studies reported a reduction in energy and CO_2 emission when comparing the system with seasonal storage to a baseline one. Real-world examples of such systems are the Drake Landing solar community in Canada [6], where a solar thermal system with borehole seasonal storage supplies space heating to more than 50 homes through a district heating network, achieving a solar fraction of 97%. The solar district heating in Crailsheim, Germany [7], with a similar centralized design principle, aims at achieving a 50% solar fraction. While some

* Corresponding author.
E-mail address: massimo.fiorentini@empa.ch (M. Fiorentini).

https://doi.org/10.1016/j.energy.2022.125464
Received 26 September 2021; Received in revised form 5 September 2022; Accepted 14 September 2022
Available online 19 September 2022

Nomenclature

ΔT	BTES charging and discharging temperature difference (°C)
δ	discrete variable associated with different BTES configurations (-)
$\dot{m}$	heat transfer fluid mass flow rate (kg/s)
η	efficiency (%)
λ	equipment cost per unit of size (€/.)
ν_{CO_2}	CO_2 emissions price (€/t)
ν_{el}	electricity price (€/kWh)
ω	annuity factor (%)
ρ	density (kg/m^3)
A_i	area of the BTES top insulation (m^2)
c_p	specific heat capacity (kWh/kg K)
D	storage depth (m)
h	BTES heat loss factor (-)
I_{CO_2}	electricity CO_2 intensity (g_{CO_2}/kWh)
I_{sol}	solar radiation intensity (kW/m^2)
J	system cost (€)
k	thermal conductivity (kW/m K)
N	optimization horizon length
n_{GHX}	number of ground heat exchangers (-)
P	power (kW)
S	solar collectors, heat pumps and chillers size (m^2, kW)
T	temperature (°C)
U_i	thermal conductivity of BTES top insulation (kW/m K)
UA	total conductance of ground heat exchangers (kW/K)
V	BTES volume (m^3)

Subscripts and superscripts

a	air
BT	BTES
c	capital
ch	chiller
CO_2	CO_2
d,cs	district cold supply
d,hs	district hot supply
el	electrical
g	ground
GHX	ground heat exchanger
hp	heat pump
i	insulation
max	maximum
min	minimum
o	operational
sol	solar
$STTS$	short-term thermal storage
th	thermal
tot	total
tr	transferred to BTES
$used$	used directly

Acronyms

BTES	borehole thermal energy storage
TES	thermal energy storage
GHX	ground heat exchanger
HTF	heat transfer fluid
MES	multi-energy systems
MPC	model predictive control
STTS	short-term thermal storage
MILP	mixed-integer linear programming

of these systems operated relatively effectively, achieving good results in terms of solar fraction, the temperature-dependent efficiency of the BTES was generally lower than expected at the design stage. This is one of the reasons that lead modern systems generally operate BTES at lower temperatures, to reduce the heat losses to the surrounding undisturbed ground. This also enables the network to operate at lower temperatures, with heat pumps employed to provide heating at the temperature required by the end-users distribution system. When short-term and seasonal thermal energy storages are implemented in newer generation thermal networks, often referred to as 5th generation district heating and cooling systems, they enable buildings to become thermal prosumers, similarly to an electrical smart grid [8], giving them the ability to contribute by storing the heat rejected from cooling operations, or generated from low-temperature solar or waste heat sources.

The optimization of the design and operation of energy systems is crucial in ensuring that their best techno-economical performance is achieved. Several computational methods have been applied to sustainable building and energy system design, as the comprehensive review in [9] presents. In particular, the review in [10] discusses the different types of optimization problems, constraints and optimization tools as well as techniques used for optimally sizing district energy systems. The energy hub concept, introduced by Geidl et al. [11] is a powerful approach that represents the interactions of several energy conversion and storage technologies, which can be combined with mathematical optimization approaches to support multi-energy systems (MES) design. Several studies employed similar methods to optimize the design process of energy systems. The importance of properly describing operational constraints when formulating the optimization of a MES was highlighted in [12], where an extension of the energy-hub approach is presented. The study in [13] employed a particle-swarm optimization approach covering both the design and operation of short-term electrical and thermal storage, with the objective of minimizing daily electricity and life cycle costs. Similarly, the paper in [14] used a mixed-integer linear programming (MILP) formulation to optimize a short-term thermal storage sizing and operation, with objective for the storage to assist solar generation to maximize self-consumption. Other papers aimed at optimizing multi-energy generation, storage and energy conversion devices sizing as distributed energy resources [15], while the study in [16] performed an energy system optimization both at building level and at a neighbourhood level, where also the district heating network investment was considered.

To predict the performance of a BTES, its thermal behaviour is generally modelled in detail using software tools such as TRNSYS [17] at both district and residential scales. At district scale, the study in [18] used TRNSYS to optimize the design of a system including a BTES, a ground-coupled heat pump and evacuated tube solar collectors in several heating-dominated locations, and the study in [19], with a similar approach, optimized a system with seasonal storage and solar generation located in Barcelona. At residential scale, an example is provided in Antoniadis et al. [20], where the design of a seasonal thermal storage combined with solar collectors was studied. The downside of the approach taken by these studies is that these modelling methods do not allow the application of numerical optimization methods, and finding the optimal solution in an iterative manner might always not be

possible. Only a few studies included seasonal thermal energy storage within a system numerical optimization framework, particularly using a BTES. For example, the paper by Prasanna et al. [21] used an energy hub approach to determine the scenarios in which the design of the system would include more thermal and electrical storage in a low-temperature district network case-study, whether Gabrielli et al. [22] proposed an optimization methodology to consider seasonal storage in a system design optimization problem that retains an hourly resolution. Wirtz at el. [23] employed a similar optimization approach, extending it to bidirectional low-temperature networks. To formulate the system design optimization as a MILP problem, these studies simplified the dynamical behaviour of the seasonal thermal storage and did not consider important factors as its temperature evolution and the consequent effect on the efficiency of the connected equipment. The study in [24] modelled the BTES behaviour as part of the optimization problem the g-function method, and this lead to a non-linear problem that was solved using a bi-level optimization framework, employing a genetic algorithm for the multi-objective design problem and a MILP approach for the operational one. The importance of more detailed modelling of thermal energy storage (TES) systems, even short-term, is highlighted in [25], where a multi-layer TES model that retains linearity is introduced by improving tracking of losses based on ambient and storage temperatures. A similarly linearized modelling approach has also been proposed for supporting operational optimization frameworks for MES, leading to analogous MILP formulations. Examples include the work presented in [26], where this approach was used to optimize the operating schedule of a combined heat and power plant to minimize the total operating and maintenance costs, or in [27], to optimize the operation of a thermal and electrical energy storage systems in a building. This approach to system operation optimization has also been proposed in recent studies with application on 5th generation district heating and cooling networks [28], or district heating networks with thermal storage [29]. Nevertheless, only a limited number of studies consider them for seasonal thermal storage. An example is provided in [30], where a model predictive control (MPC) approach designed for the aforementioned Drake Landing solar community was proposed, or in [31], where the operational optimization of a case study featuring an anergy grid with a low-temperature BTES is presented. Most of these design and operation optimization studies focused on the economical optimization of energy systems, and the impact of other parameters such as the CO_2 price was rarely investigated and considered as part of the uncertainties to be included in the optimization approach, such as the study in [32], that proposed a multi-objective optimization that incorporates uncertain parameters by applying the concept of minmax optimization for designing sustainable energy supply systems, or the one in [33], which focused on the optimal deployment of Power-to-Hydrogen conducting a comprehensive uncertainty analysis on technology parameters and boundary condition, including CO_2 price.

Furthermore, the relationship between design and operational optimization is particularly important when thermal energy systems are studied as highlighted in [34], and this should also be considered in design optimization procedures. This consideration is particularly relevant for energy systems with seasonal thermal energy storage, where the operational implications on the system optimal design have not yet been studied in detail. The goal of this study is therefore to develop an energy system design optimization framework for district heating and cooling systems integrating a BTES, enabling a rapid estimation of the optimal sizing and combination of technologies under different boundary conditions. The application of this approach to a case study district uncovers combined optimal sizing and operation trends as function of different boundary conditions, which were not reported in previous studies.

1.1. Research gap and contribution

Most of the studies that propose a design optimization of seasonal storage tackle the problem with iterative methods, using detailed modelling and simulation tools (e.g. the district level study in [18], or the residential scale one in [20]), which are not suitable for numerical optimization, or employ significantly simplified models (e.g. a storage capacity with constant losses) to enable the application of optimization methods to determine the best seasonal storage and supporting equipment capacity (e.g. the optimal storage scenario analysis in [21] or the recent multi-energy system optimization in [23]). Nevertheless, the optimal size of the seasonal thermal energy storage and its operational conditions (e.g. temperature evolution) are linked. The storage operating conditions also affect the efficiency of the equipment connected to it. This paper, therefore, proposes a non-convex optimization programming formulation that, differently from the studies available in the literature, can consider:

- The influence of operational decisions such as the initial temperature of the BTES storage temperature swing on the total capacity of the storage and thermal losses of the storage.
- The connection between the volume of the BTES storage and its maximum heat transfer rate.
- The effect of the temperature difference between heat transfer fluid (HTF) and storage on the heat transfer rate when the storage is charged or discharged and as well as on the efficiency of the connected heat pump or chiller.
- The impact of boundary conditions such as the availability of solar thermal generation, the CO_2 intensity of the grid electricity consumed, the ratio between heating and cooling (rejected waste heat) demand, and price of direct CO_2 emissions.

The proposed formulation aims at demonstrating how the optimal equipment sizing and key operational conditions of the storage (e.g. its temperature swing, the temperature difference imposed by the conversion equipment) and sizing of supporting systems (e.g. solar thermal collectors) vary in function of different boundary conditions, under the objective of minimizing operational CO_2 emissions and life cycle cost.

2. Energy system design optimization

This study considers a generic district heating and cooling system configuration with centralized energy generation and storage. Seasonal thermal energy storage is achieved via a cylindrical BTES, with an in-parallel plumbing configuration. In line with the requirement of avoiding the use of fossil fuels for heat generation, electricity is assumed to be the only primary source of energy for the provision of on-demand heating and cooling. It therefore is assumed that the buildings' cooling demand can be met by two chillers, one that rejects the waste heat in a BTES and a second one that uses the ambient air as a sink. The heating demand can be met by two heat pumps, also using the BTES and the ambient air as sources. As the total heating demand of the site might differ significantly from the cooling one, so an additional solar thermal heat source can be considered in the design optimization of the system. The solar thermal system is assumed to be able to provide heat either directly to the district heating system, or store it into the BTES. It is assumed that the solar thermal collectors are coupled with a buffer tank large enough to absorb daily fluctuations in energy generation.

Fig. 1 shows the described setup operated in cooling mode and BTES charging, as well as in heating mode and BTES discharging.

The design optimization of the energy system considered in this study has the objective of fulfilling the thermal energy demand of the district, while minimizing the yearly cost of the energy system. This cost comprises of capital and operational components, with an additional operational cost associated with the CO_2 emissions of the system. The CO_2 emissions price is used in this study as a key decision variable to influence the system design and configuration.

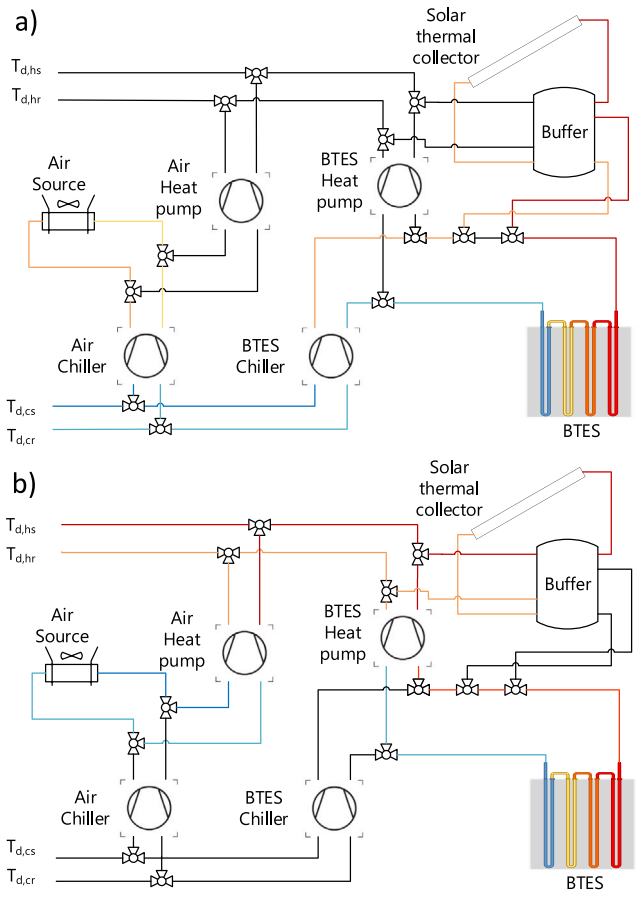

Fig. 1. Case study operating in (a) cooling mode and BTES charging, and in (b) heating mode and BTES discharging.

2.1. Input data

The weather conditions (solar radiation I_t and ambient temperature T_a), CO_2 intensity profile of the electricity (I_{CO_2}), and heating and cooling demand profiles ($P_{load,heat}$ and $P_{load,cool}$) are the primary sets of inputs to the optimization problem, which returns the optimal system design in terms of technology sizing and operational conditions. The input weather, CO_2 intensity and demand data are provided for a year with an hourly resolution, and they are assumed not to change along the lifetime of the system.

2.2. Decision variables

The optimization returns, under defined boundary conditions, the best sizing and operational decision variables for the energy system considered, assuming that the defined heating and cooling demand must be met. These decision variables include:

i. The optimal equipment sizing, including the heat pump and chillers thermal capacity ($S_{hp\_BT}, S_{ch\_BT}, S_{hp\_a}, S_{ch\_a}$), solar thermal collectors area (S_{sol}), and volume of the BTES (discretized, V_j).
ii. The optimal temperature difference between fluid and BTES in charging with the chiller and discharging with the heat pump (ΔT_{ch} and ΔT_{hp} respectively) and optimal initial temperature of the BTES temperature swing ($T_{BT,init}$).
iii. The fraction of heating and cooling demand provided, at each time step k, by the solar generation (P_{th,sol_used}), by the heat pump and chiller connected to the BTES (P_{th,hp_BT}, P_{th,ch_BT}) or by the air-source heat pump and chiller (P_{th,hp_a}, P_{th,ch_a}).
iv. The fraction of solar generation, at each time step, stored in the BTES (P_{th,sol_tr}).

The electrical power consumption of the energy system ($P_{el,tot}$) at each time step is calculated, as the sum of the contribution from all the heat pumps and chillers considered, to estimate the operational costs and CO_2 emissions to be included in the optimization objective function. The electrical power consumption of circulation pumps is not considered in this study.

2.3. Constraints

The optimization problem for the energy generation, conversion and storage equipment is subject to constraints that affect both design and operational variables. Solar collectors area, as well as the chillers and heat pumps capacities, were considered as continuous variables. The BTES sizing was discretized as the properties of the storage change with the storage volume, such as the thermal losses and the possibility to transfer heat.

2.3.1. Seasonal storage

The BTES is assumed to be cylindrical, with uniformly distributed boreholes, and employing an in-parallel plumbing configuration such that it can be modelled as a single capacitance. Its dynamical thermal response is therefore described as a lumped-capacitance model, employing the steady-state equation proposed in [35] to calculate the thermal losses around the storage. The heat losses occur through the top insulation, which has an area equal to A_i and a U-value U_i, through the uninsulated part of the BTES. These losses are expressed as a function of the storage depth, storage aspect ratio and ground thermal conductivity. This simplified model was compared to a TRNSYS 18.02 equivalent one, using a TRNSYS TYPE based on the TRNSBM [36] package. This comparison showed an acceptable accuracy of the simplified BTES model, with a slight overestimation of the storage thermal efficiency, as show in Fig. A.13. While this model is deemed suitable for the purpose of this study, differently formulated linear time-invariant models could also be employed. The set of storage sizes contains n_j elements, each corresponding to a storage volume V_j. To linearly model the relation between the maximum heat transfer rate and the temperature difference between the ground and the HTF, an equivalent UA_j coefficient is calculated for each BTES configuration, assuming forced internal convection in the ground heat exchanger (GHX) and a constant borehole wall temperature that is equal to the overall BTES temperature. In this study the value of this UA coefficient was identified by simulating the BTES in design conditions in TRNSYS. This was achieved, as presented in [37], by minimizing the root-mean-square error (RMSE) between the predicted heat transfer of the BTES and the one simulated using the TRNSYS model under the same boundary conditions. As it assumed that the storage keeps the same aspect ratio (diameter equal to depth) when scaled, the heat loss factor h for the proposed steady-state heat loss formulation is the same in each of the various sizes considered.

The BTES cost (J_{BT}) in each scaling option is obtained from the total drilling length, calculated as the product of the number of GHXs and their depth, multiplied by a drilling price per meter (λ_{GHX}) and an annuity factor (ω_{BT}). Furthermore, the heat transfer is constrained in each storage configuration by the total UA value (UA_j) of the ground heat exchangers and temperature difference between HTF and storage ($\Delta T_{ch}, \Delta T_{dis}, T_{sol} - T_{BT}$). The storage temperature evolution and constraints in each configuration j are presented in Eq. (1):

$$\begin{cases} T_{BT}(k+1) = T_{BT}(k) + \frac{\Delta t}{\rho_g c_{p,g}} V_j (P_{th,ch\_BT}(k) - P_{th,hp\_BT}(k) + \\ \qquad P_{th,sol\_tr}(k) - U_i A_{i,j} (T_{BT}(k) - T_a(k)) \\ \qquad - k_g h \frac{D_j}{2} (T_{BT}(k) - T_g)) \\ P_{th,ch\_BT}(k) <= UA_j \Delta T_{ch} \\ P_{th,hp\_BT}(k) <= UA_j \Delta T_{hp} \\ P_{sol,tr}(k) <= UA_j (T_{sol} - T_{BT}(k)) \\ J_{BT} = D_j n_{GHX,j} \lambda_{GHX} \omega_{BT} \end{cases} \quad (1)$$

where T_{BT} is the temperature of the storage, T_a the ambient temperature, T_{sol} the supply temperature of the solar system and T_g the undisturbed ground temperature. ρ_g and $c_{p,g}$ are the density and specific heat capacity of the ground. Each one of the BTES designs is activated by its respective Boolean variable included in the array $\overline{\delta} = [\delta(1), \ldots, \delta(n_j)]$, where the first variable $\delta(1)$ is associated with the system configuration without a BTES. The fact that only one BTES design can be employed in the optimal energy system design is ensured by the constraint in Eq. (2):

$$\sum_{j=1}^{n_j} \delta(j) = 1 \tag{2}$$

The operating temperature range of the storage is defined by the constraint in Eq. (3):

$$T_{BT}^{min} \leq T_{BT}(k) \leq T_{BT}^{max} \tag{3}$$

Similarly, the storage initial temperature is constrained within a temperature range (Eq. (4)):

$$T_{BT,init}^{min} \leq T_{BT}(1) \leq T_{BT,init}^{max} \tag{4}$$

To ensure that the energy content of the BTES at the beginning and end of the year are equal, the storage temperature at the last time step N must be equal to the temperature at the initial one (Eq. (5)).

$$T_{BT}(N) = T_{BT}(1) \tag{5}$$

2.3.2. Heat pump and chiller

To enable the optimization to choose the best source between the BTES and the air for providing heating and cooling, the sizing and the operation of the two heat pumps and chillers are considered as variables. The thermal capacity of each heat pump is constrained between zero and the maximum heating demand to the plant (Eq. (6)):

$$0 \leq S_{hp\_a}, S_{hp\_BT} \leq P_{th,load\_heat}^{max} \tag{6}$$

Similarly the chillers maximum capacity is constrained by the maximum cooling demand (Eq. (7)):

$$0 \leq S_{ch\_a}, S_{ch\_BT} \leq P_{th,load\_cool}^{max} \tag{7}$$

The heat generation at each time step k of the heat pumps is consequently constrained by the thermal capacity of the equipment:

$$0 \leq P_{th,hp\_a}(k) \leq S_{hp\_a} \tag{8}$$

$$0 \leq P_{th,hp\_BT}(k) \leq S_{hp\_BT} \tag{9}$$

Similarly for cooling provided the chillers is constrained by their capacity:

$$0 \leq P_{th,ch\_a}(k) \leq S_{ch\_a} \tag{10}$$

$$0 \leq P_{th,ch\_BT}(k) \leq S_{ch\_BT} \tag{11}$$

The electrical consumption of the heat pumps and chillers is derived by dividing, at each time step, their thermal output by their relative COP (Eq. (12)):

$$P_{el}(k) = P_{th}(k)/COP(k) \tag{12}$$

As the COP of the air-source heat pump and chiller can be determined beforehand and does not need to be computed as part of the optimization, the non-linear relationship in Eq. (13), based on a constant exergy efficiency, is used:

$$\begin{cases} COP_{hp\_air}(k) = 0.5 \frac{T_{d,hs}}{T_{d,hs} - (T_a(k) - \Delta T_{hp,a})} \\ COP_{ch\_air}(k) = 0.5 \frac{T_{d,cs}}{(T_a + \Delta T_{ch,a}) - T_{d,cs}} \end{cases} \tag{13}$$

where $T_{d,hs}$ and $T_{d,cs}$ are the district supply hot and cold temperatures, $\Delta T_{hp,a}$ and $\Delta T_{ch,a}$ are the temperature differences between the HTF and the air in design conditions, to enable the heat exchangers to operate efficiently (all temperatures are evaluated in K in Eq. (13)). The values of these two temperature differences were considered constant in this study and equal to 10 K.

The COP heat pump and chiller connected to the BTES depends on the storage temperature and, as it is part of the optimization process, cannot be determined beforehand. To enable numerical optimization of this design and operational problem, a linearized formulation of the inverse of the COP of the chiller charging the BTES and the COP of the heat pump discharging it are employed, as presented in Eq. (14).

$$\begin{cases} COP_{ch\_BT}^{-1}(k) = a_{ch}(T_{BT}(k) + \Delta T_{ch}) + b_{ch} \\ COP_{hp\_BT}^{-1}(k) = a_{hp}(T_{BT}(k) - \Delta T_{hp}) + b_{hp} \end{cases} \tag{14}$$

Assuming a linearization of the relationship in Eq. (13) undertaken in the expected operation range of the equipment, the coefficients a_{ch}, b_{ch}, a_{hp} and b_{hp} in Eq. (14) can be determined. As the electrical consumption of the equipment is the product of the linearized COP^{-1} and P_{th}, the optimization problem is non-convex with quadratic constraints, and can be solved by modern solvers such as Gurobi [38].

2.3.3. Solar thermal system

It is assumed that the solar panels generate heat at a constant efficiency and that they are coupled with a buffer tank capable of shifting part of the daily generation to the night, supporting the assumption of optimizing the system with a daily resolution and averaging the input data over a 24 h period. The solar thermal collector area S_{sol} is constrained by the maximum available space (15):

$$0 \leq S_{sol} \leq S_{sol}^{max} \tag{15}$$

The heat generation of the solar panels $P_{th,sol}$ can be calculated at each time step as in Eq. (16):

$$P_{th,sol}(k) = \eta_{sol} I_{sol}(k) S_{sol} \tag{16}$$

where the η_{sol} is the efficiency of the solar collectors and I_{sol} is the solar radiation. The short-term thermal storage (STTS) is sized to shift half of the maximum daily solar generation (Eq. (17)):

$$S_{STTS}(k) = \eta_{sol} I_{sol}^{max} S_{sol} \Delta t/2 \tag{17}$$

At each time step, the sum of the solar generation used directly by the district heating system and the solar heat transferred to the BTES must not exceed the total generation of the solar collectors, as enforced by the constraint in Eq. (18).

$$P_{th,sol}(k) \leq P_{th,sol\_tr}(k) + P_{th,sol\_used}(k) \tag{18}$$

2.3.4. Plant thermal balance

At plant level, the heating and cooling loads must be met at each time step, using the available energy resources. It is also assumed that simultaneous heating and cooling demand can be met within a given time-step, and the net demand of the district can be calculated and averaged over each day. The heating load can be met by using solar energy directly, as well as by the air-source and BTES heat pumps. Similarly, the cooling demand can be satisfied by the air source and BTES chillers (Eq. (19)).

$$\begin{cases} P_{load,heat}(k) = P_{th,hp\_BT}(k) + P_{th,hp\_a}(k) + P_{th,sol\_used}(k) \\ P_{load,cool}(k) = P_{th,ch\_BT}(k) + P_{th,ch\_a}(k) \end{cases} \tag{19}$$

2.4. Objective function

The objective function of the optimization problem represents the total annual cost of the energy system J, which includes a capital component (J_c), and operational components related to energy consumption ($J_{o,e}$) and CO_2 emissions (J_{o,CO_2}).

The annual capital cost is expressed as the sum of the equipment cost (Eq. (20)):

$$J_c = \omega_{eq}(\lambda_{hp}(S_{hp\_BT}+S_{hp\_a})+\lambda_{ch}(S_{ch\_BT}+S_{ch\_a})+\lambda_{sol}S_{sol}+\lambda_{ST}S_{ST})+J_{BT} \quad (20)$$

where each λ is the equipment price (i.e. capital cost per unit of size for each of the considered equipment) and ω_{eq} is the annuity factor. For simplicity and ease in interpreting the results, interest rates and respective discounting were not considered in this study.

The operational cost of energy consumption depends on the total electrical energy consumption of the system, which is calculated at each time as shown in Eq. (21).

$$P_{el,tot}(k) = P_{el,hp\_BT}(k) + P_{el,ch\_BT}(k) + P_{el,hp\_a}(k) + P_{el,ch\_a}(k) \quad (21)$$

Assuming v_{el} as a constant electricity price per kWh, the operational cost related to the energy consumption $J_{o,e}$ is calculated as in Eq. (22).

$$J_{o,e} = \sum_{k=1}^{N}(P_{el,tot}(k))v_{el}\Delta t \quad (22)$$

Similarly, integrating the product of electricity consumption and CO_2 intensity at each time step k and considering a constant CO_2 price, the total CO_2 emissions operational cost J_{o,CO_2} is calculated as in Eq. (23).

$$J_{o,CO_2} = \sum_{k=1}^{N}(I_{CO2}(k)P_{el,tot}(k))v_{CO_2}\Delta t \quad (23)$$

3. Implementation

This section presents the application of the methodology described in Section 2 to a case study district heating and cooling system serving the Empa campus in Dübendorf, Switzerland.

3.1. Input data

The input data employed to analyse the case study refers to the Empa campus, and includes weather conditions (solar radiation and ambient temperature), CO_2 intensity profile of the electricity, and heating and cooling demand profiles. The heating and cooling demand data used in this study were sourced from the operational history of the Empa campus, which includes 35 buildings of different use (e.g. office, laboratory, etc.) and requires both process and space heating and cooling. The thermal energy, currently generated with a natural gas boiler and a chiller, is distributed to the buildings using heating and cooling networks. As simultaneous heating and cooling demand is assumed to be instantaneously met, the net demand of the campus was calculated and averaged over each day. This results in the thermal load profile shown in Fig. 2, where a positive power represents net demand for heating and negative for cooling. Here it can be noticed that the maximum district heat demand was approximately 3.3 MW and the maximum cooling demand approximately 1 MW. The weather file Dübendorf TMYx [39] was used to derive the ambient temperature and solar radiation profiles, both re-sampled with averaging at a daily resolution. The reference CO_2 equivalent intensity profile for Switzerland was sourced from [40]. The profile of these boundary variables is presented in Fig. 2, where for both variables, profiles and distribution are shown. All the datasets are one year long, with a daily resolution. They begin in May, aligning with the beginning of the cooling (BTES charging) period.

Table 1
BTES construction parameters.

Parameter	Value
Borehole diameter (m)	0.14
U-pipe diameter (m)	0.04
U-pipe thickness (m)	0.0032
U-pipe thermal conductivity (W/m K)	0.35
U-pipe shank spacing (m)	0.06
Filling thermal cond (W/m K)	0.6
Contact resistance pipe/filling (m K/W)	0.02
Heat conductivity ground layer (W/m K)	2.4
Volumetric heat capacity ground layer (kJ/K m^3)	2200
Initial ground temperature (°C)	12

Table 2
BTES discrete sizing options considered by the optimization.

Bool var.	Diam./Depth (m)	Volume (×10^3 m^3)	UA (kW/K)	n_{GHX}
$\delta(1)$	53.4	119.2	22.5	158
$\delta(2)$	61.2	179.6	33.8	207
$\delta(3)$	70.0	269.4	50.6	271
$\delta(4)$	80.1	404.1	76.0	355
$\delta(5)$	91.7	606.1	113.9	466
$\delta(6)$	0	0	0	0

3.2. Case study energy system

The heating network considered supplies heat at 65 °C ($T_{d,hs}$) and the cold network at 6 °C ($T_{d,cs}$), while the solar thermal system is assumed to provide heat to the network and to the BTES at 70 °C. The properties of the ground and the GHXs used for the BTES are summarized in Table 1.

As part of the system design optimization, different BTES sizes are considered with the same cylindrical shape and aspect ratio. In particular, the BTES depth and diameter are assumed to be equal, to minimize its thermal losses. Therefore the heat loss coefficient h was assumed to be equal to 21.2, as suggested in [35]. The thermal conductivity of the BTES top insulation U_i was assumed to be equal to 0.14 kW/m K. As the GHXs are assumed to be uniformly distributed, an BTES increase in size implies the installation of more and deeper boreholes. The length and number of boreholes are thus changed according to the total volume of the BTES storage. The base design used for determining the characteristics of the BTES was derived from [41]. To satisfy the heating and cooling demand presented in Section 2.1, five BTES configurations were considered by the optimization framework, in addition to the case without a BTES. The annual cost of the BTES was calculated assuming a lifetime of 60 years, with the construction characteristics presented in Table 2.

The BTES cost was calculated, as presented in Section 2, from the GHX cost of installation per meter (λ_{GHX}), which was assumed to be 66 €/m [42]. The undisturbed ground temperature was assumed to be equal to 12 °C, and the minimum (T_s^{min}) and maximum (T_s^{max}) operating temperatures of the storage were set at 6 °C and 65 °C respectively. The initial temperature range of the BTES ($T_{s,init}^{min}$, $T_{s,init}^{max}$) was constrained between 8 °C and 30 °C, as typical heat pump-driven BTES systems in balanced operation would have a lower operation boundary in a similar range, as reported in [43]. A limit on the maximum initial temperature of the storage has also implications on how many years the BTES needs to operate in an unbalanced manner, charging more heat in summer than extracting in winter to reach a higher average storage temperature. The parameters and prices of the heat pumps, chillers and solar collectors are summarized in Table 3. For this equipment, a lifetime of 20 years was assumed.

The efficiency of the collectors (η_{sol}) was assumed to be equal to 0.65. The STTS volume which is assumed to be proportional to the collector area was assumed to have a cost (λ_{ST}) equal to 9 €/kWh [33]. Considering the aforementioned networks operating conditions, the

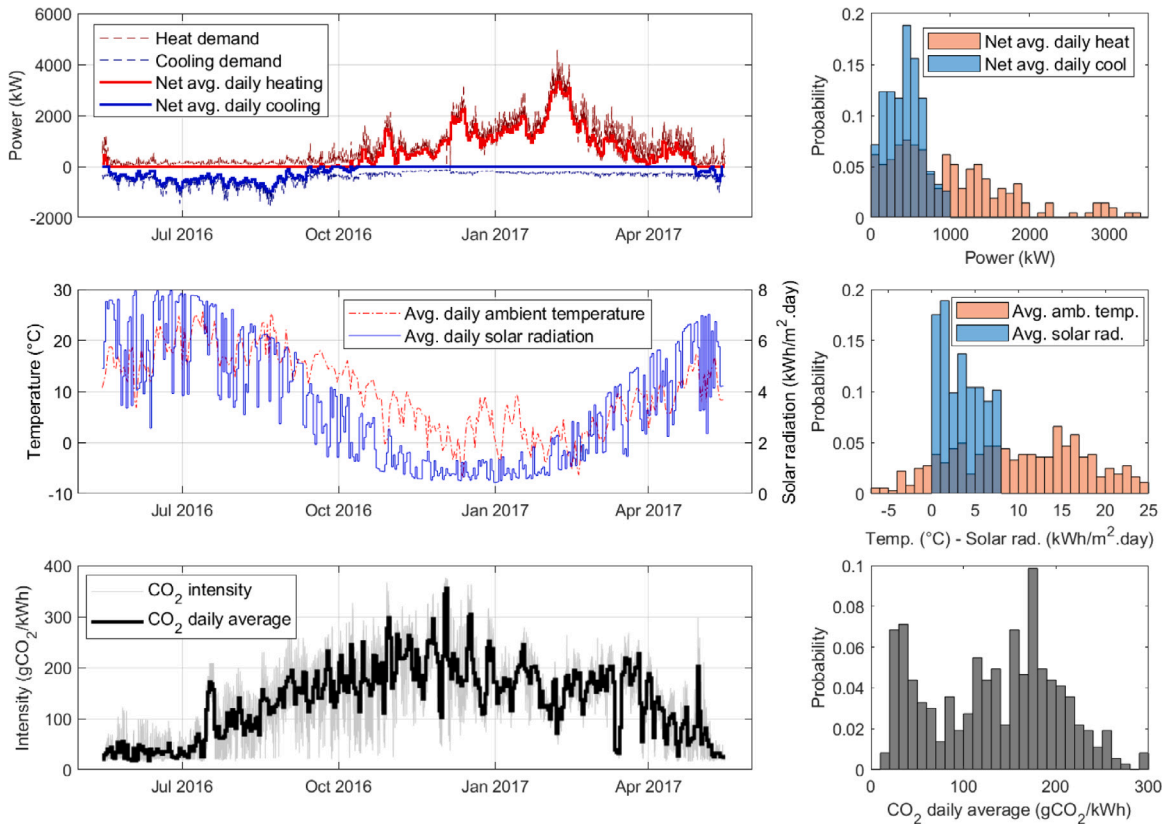

Fig. 2. Input data used for the optimization case study, including the heating and cooling demand of the Empa campus (top), ambient temperature and solar radiation datasets (middle) and CO_2 equivalent emissions intensity of the Swiss electricity grid [40] (bottom). The figures on the left present the input data profiles, the figures on the right the input data distribution.

Table 3
Heat pumps, chillers and solar thermal collectors price and maximum size.

Parameter	λ	S^{max}
S_{sol}	500 €/m^2	10^4 m^2
S_{hp_BT}, S_{hp_a}	576 €/kW	3307.4 kW
S_{ch_BT}, S_{ch_a}	576 €/kW	974.5 kW

charging COP ($COP_{ch\_BT}(k)$) was linearized in this study for a rejection temperature between 25 and 65 °C, with a cooling supply temperature equal to 6 °C ($T_{d,cs}$), resulting in coefficients a_{ch} and b_{ch} equal to $5.52 \cdot 10^{-3}$ and $-5.14 \cdot 10^{-3}$ respectively. The discharging COP ($COP_{hp\_BT}(k)$) was linearized assuming an inlet temperature between −5 and 25 °C and a heating supply temperature equal to 65 °C, resulting in coefficients a_{hp} and b_{hp} equal to $-5.92 \cdot 10^{-3}$ and 0.3844 respectively.

As only operational CO_2 emissions are considered in this study, no emissions are associated with the heat generation of the solar thermal collectors. The electricity price v_{el} was assumed to be constant at 0.156 €/kWh [44]. A range of CO_2 prices from 50 €/t to 500 €/t was tested. As a reference, the lower limit is approximately the current EU carbon price [45], while direct extraction of CO_2 from the atmosphere is estimated to cost between 110 €/t and 280 €/t [46].

The optimization was performed with a daily resolution (Δt equal to 24 h) and a yearly horizon (N equal to 365 days). To avoid numerical issues when solving the optimization problem, the costs in the objective function were converted to k€.

3.3. Testing procedure

To evaluate the effect on the optimal design and operation of the energy system of boundary conditions such as the ratio of cooling demand in relation to the heating one, and the seasonal variation in CO_2 intensity of the electricity used, four testing scenarios were considered.

Considering the heating and cooling demand ratio, the following scenarios were considered:

- standard cooling demand profile, as presented in Section 3.2.
- increased cooling demand profile, where the cooling is three times larger than in the standard scenario, and therefore of approximately the same order of magnitude as the heating demand.

The current Swiss seasonal CO_2 intensity profile follows a sinusoidal trend [40], with lower intensity in summer compared to the one in winter. To represent the current and a higher penetration of renewable energy in the summer electricity generation, the following CO_2 scenarios were considered:

- standard CO_2 intensity profile, as presented in Section 3.2.
- modified CO_2 intensity profile, where the summer CO_2 intensity is 1/3 of the standard scenario, simulating a higher relative difference between intensity in summer and winter.

The optimization was performed in each scenario considering different CO_2 prices in the aforementioned range, to assign more or less priority to the CO_2 emissions. The results from this set of optimizations were replicated with and without the possibility to include solar thermal collectors to support the energy system.

A machine with an 8th generation Intel i7 processor (6 cores) and 32 GB of RAM was used to conduct this study. The optimization problem was formulated in Matlab R2020b, using the Yalmip toolbox [47] and Gurobi v9.1 [38] as a solver. The computational time to find the optimal solution changed with the optimization scenario and boundary conditions considered, with a maximum of approximately one hour.

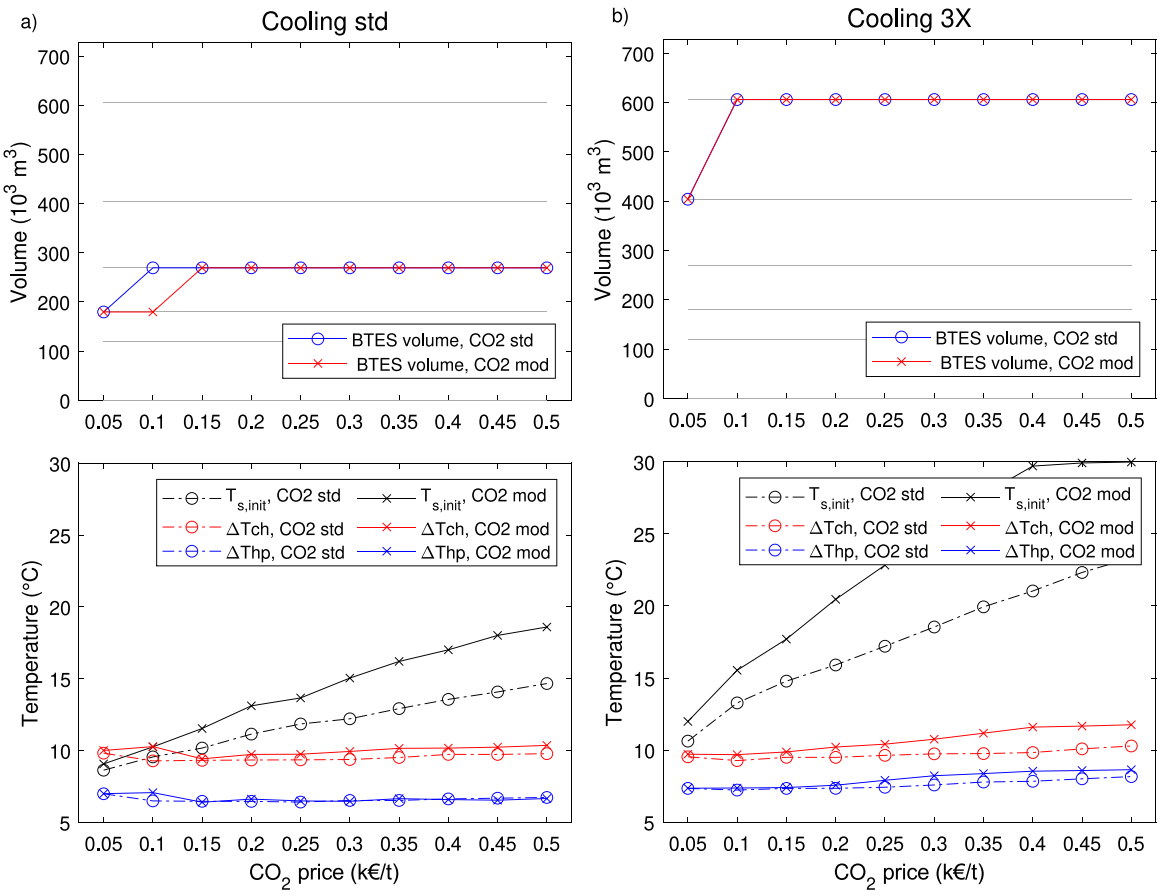

Fig. 3. Optimal BTES size (top) and operation (bottom) as a function of the CO_2 cost, in the (a) standard cooling demand and (b) increase cooling demand (3X) scenarios.

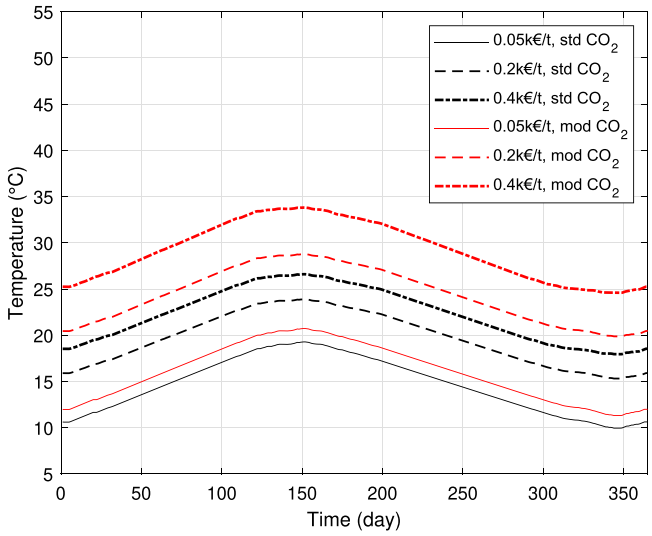

Fig. 4. Optimal temperature profile of the BTES in the increased cooling demand (3X) scenario, without integration of solar generation, using different CO_2 prices and standard (std) and modified (mod) CO_2 intensity profiles.

4. Results and discussion

In this section, the results from the application of the methodology presented in Section 2 to the selected case described, following the boundary conditions scenarios presented in Section 3.3, are presented. First, the results from the system design optimization without the possibility to integrate solar generation are described, to highlight the effect of the boundary conditions specifically on the BTES design and its operation. In a second subsection, the results from the same optimization, including the possibility to include solar thermal collectors, are shown.

4.1. Borehole thermal energy storage only results

The results from the BTES optimization without an additional solar heat source show that in the standard cooling demand scenario,

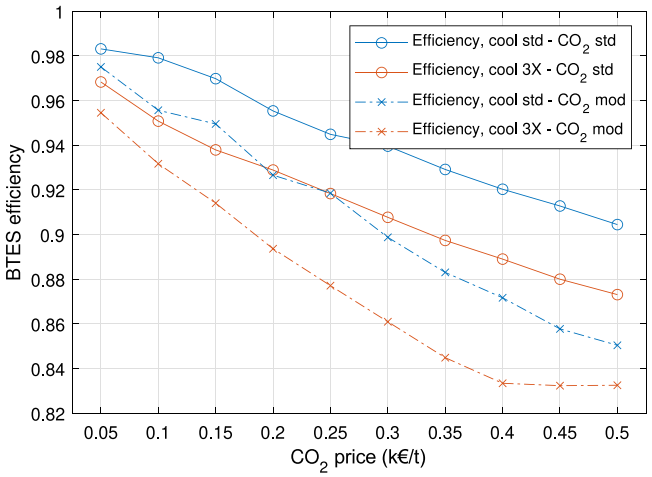

Fig. 5. Efficiency of the BTES in the various optimal system solutions found for different CO_2 costs, without integration of solar generation.

seasonal storage is useful, but with a limited volume, as shown in Fig. 3a. This is mostly because the cooling and the heating demand are unbalanced in this case, and only a portion of the latter can be covered using the BTES as the rejected heat from cooling operations is limited. It is noticeable from the operational results in the same figure that the increase in CO_2 emissions price has the effect of increasing the initial storage temperature, as well as a slightly higher temperature difference in charging (ΔT_{ch}) to enable a higher heat transfer rate to the storage. This results in a generally higher operating temperature of the BTES. This behaviour is even more evident in the modified CO_2 intensity profile scenario, as the benefits from gaining efficiency in winter, even if some is lost in summer, are even more pronounced. This is also visible in Fig. A.14a, where the overall system efficiency in heating and cooling is presented. As with a higher CO_2 price the temperature of the BTES increases, the efficiency of the cooling operations decreases for an increase in efficiency in heating. This can be observed in more detail in Fig. A.15, where the distribution of the COP of the air-source and BTES-source heat pumps and chillers for two CO_2 prices is presented. The increase in CO_2 price mainly affects the efficiency of the BTES-source heat pump and chiller, increasing the first and lowering the second. Observing the optimization results in Fig. 3b, which presents the scenario with increased cooling demand, it can be seen that the optimal BTES size is the largest in almost all CO_2 emissions prices, in both CO_2 emissions profile scenarios considered. In this increased cooling demand scenario, the optimal BTES initial temperature increases with the CO_2 emissions price even more than in the standard cooling demand scenario, particularly with the modified CO_2 emissions profile as a boundary condition.

This effect can also be seen in Fig. 4, where the yearly seasonal temperature swing of the BTES in the increased cooling demand scenario is presented. Here it can be noticed that the gradual increase in the BTES temperature swing, for equal CO_2 emissions price, is more pronounced when the modified CO_2 emissions profile was used as a boundary condition (red lines).

This increase in operating temperature, while being beneficial to the discharging COP of the heat pump, leads to a lower efficiency of the BTES, as shown in Fig. 5. As the operating temperature is fluctuating around the undisturbed ground temperature when the CO_2 emissions price is the lowest, the thermal losses are expected to be minimal. With higher CO_2 price, the storage efficiency decreases but remains around 80%.

In Fig. 6 the fraction of cooling provided by the chiller charging the BTES, and of the heat pump that uses the BTES as a source, are presented. As expected by the sizing and operational results, higher CO_2 emissions prices lead to higher fractions of rejected heat from cooling operations absorbed by the BTES. While comparing Fig. 6a with Fig. 6b, it can be seen that at high CO_2 prices the standard cooling demand – and therefore rejected heat – limits the possibility to cover a larger heating demand fraction. With an increased cooling demand (Fig. 6b) a slightly smaller low-temperature BTES is the best solution at the lowest CO_2 price (see Fig. 3), but as the CO_2 price increases, the larger BTES at a higher operating temperature enables almost all the rejected heat from the cooling operations to be absorbed.

The optimal system design solutions, as shown in Fig. 7, form different Pareto fronts depending on the scenario. The scenarios with the standard cooling profile (black lines) present a relatively narrow range for system optimization possibilities to reduce emissions. Compared to a base system without BTES, in the case of the standard CO_2 profile, this emissions reduction ranges from 4.1 to 6.7%. The modified CO_2 profile enables a slightly larger emissions reduction opportunity, from 3.9% to 8.1%. This is achieved with a yearly cost (excluding the CO_2 emissions cost), ranging from 0.3% lower to 0.3% higher. The scenario with the increased cooling demand profile (red lines) offers a significantly larger emissions reduction opportunity which, in the best case (modified CO_2 profile), ranges from 9.8% to 27.1%, with an annual cost from 0.6% lower to 1.5% higher than the system without a BTES.

4.2. Borehole thermal energy storage and solar thermal results

In this second optimization result set, in addition to the BTES, the possibility to install a solar thermal array to support the energy system was also considered. As it can be observed from the sizing and operational results in Fig. 8, the solutions found for the standard cooling demand profile (Fig. 8a) and the increased one (Fig. 8b) show that above a defined carbon price (0.1 k€/t and 0.15 k€/t respectively) including a solar thermal source becomes economical advantageous as an addition to the waste heat recovered from the cooling operations. In both figures it is noticeable that, once it becomes feasible, the optimal size of the collector array increases as expected with the CO_2 price, and the heat pump size slightly decreases as some of the heating demand can be met directly by the solar generation. As expected, in the standard cooling demand profile scenario (Fig. 8a) the optimal size of the solar collectors' array is larger than the one calculated in the increased cooling demand profile scenario (Fig. 8b), but with a relatively smaller supporting BTES. The CO_2 intensity profile has also an impact on the optimal sizing of the solar array. A modified CO_2 intensity profile favours the rejection of heat of cooling operations leads to smaller optimal solar array sizes for the same CO_2 price. At the same time, above the 0.1 k€/t and 0.15 k€/t thresholds, the operation of the BTES changes from low to high-temperature, as more heat becomes available from solar collectors in summer at elevated temperatures and without direct CO_2 emissions. This can be seen from the initial storage temperature in the bottom graphs (black lines) of Fig. 8a and Fig. 8b. As a note, removing the upper boundary constraint on the initial temperature, the optimization lead to higher initial operation temperatures, in the order of 40 to 50 °C depending on the CO_2 price. In order to achieve this high temperature, it would require years of unbalanced operation or oversizing of the solar system, which might have economical implications. Together with the increase in operating temperature, the charging temperature difference to store the waste heat from the cooling operations decreases, and the discharging one increases, to enable a higher heat transfer rate.

The effect of the CO_2 price on the BTES optimal temperature profile can also be seen in Fig. 9 where some of the results for the standard cooling scenario are presented. In this figure the difference between the optimal low-temperature solution for a low CO_2 price can be easily distinguished from the significantly higher temperature operation of the BTES supported by solar generation at higher CO_2 prices. It can also be noticed that the temperature profiles associated with a CO_2 price of 0.4 k€/t are slightly lower than the ones associated with 0.2 k€/t, as

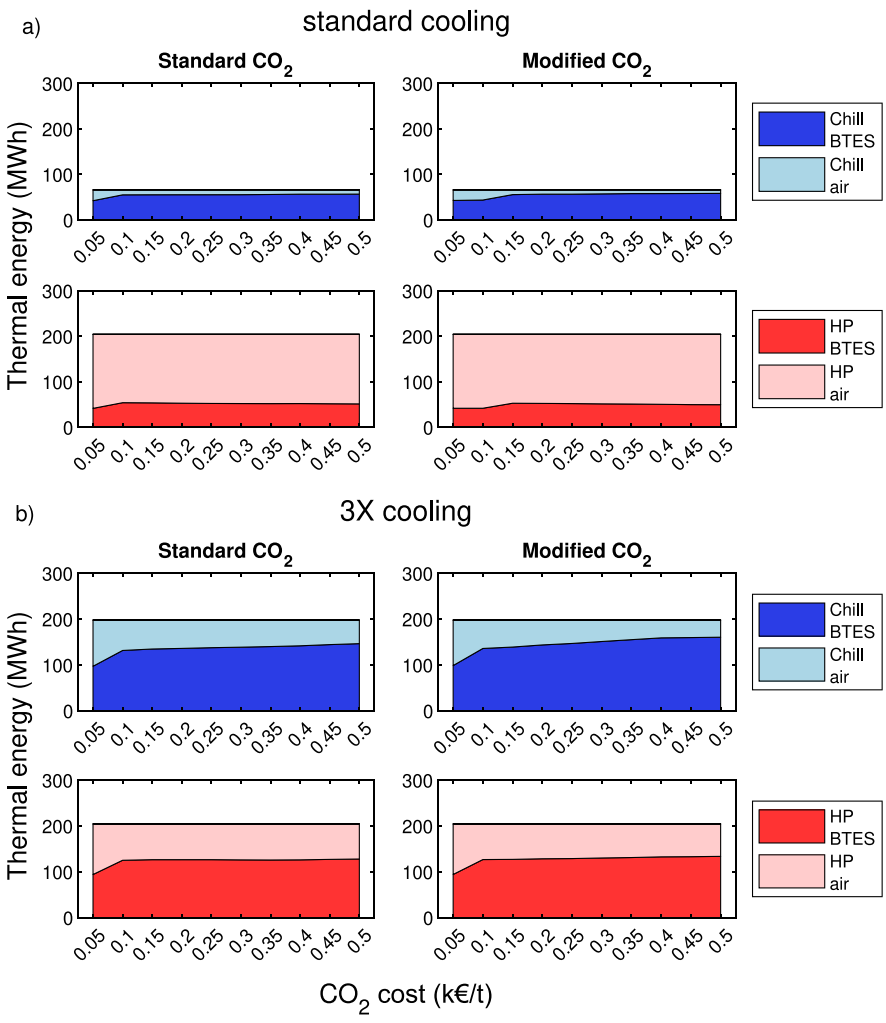

Fig. 6. Heating and cooling energy provided by the air-based or BTES-connected heat pump and chiller as function of the CO_2 cost, in (a) standard and (b) increased cooling (3X) scenarios, without integration of solar generation.

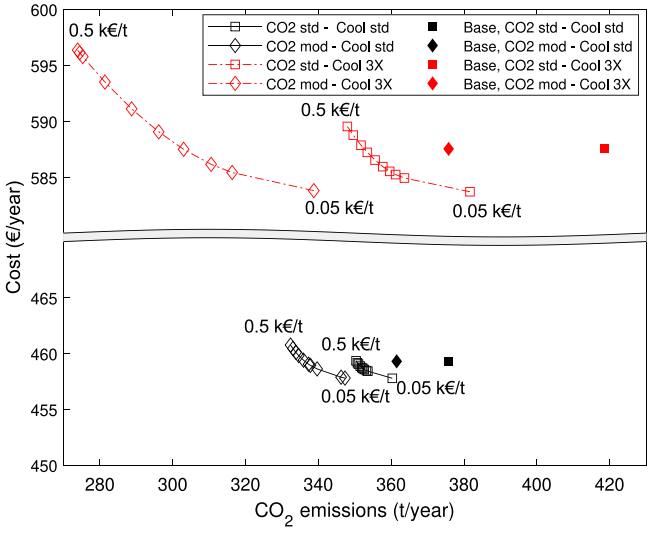

Fig. 7. Optimal system solutions under the different CO_2 intensity profile (square and rhomboidal markers) and cooling demand scenarios (black and red lines), without integration of solar generation. The "base" setup, without a BTES, is presented with a filled marker for each scenario.

the optimal BTES size at a higher CO_2 price is larger. Differently from the results obtained without solar generation, the CO_2 intensity profile has a smaller effect on the optimal design and operation solution of the BTES because the solar thermal generation has no direct impact on the electricity consumption, as shown in Fig. 9.

The efficiency of the BTES decreases as the operating temperature increases with the installation of a solar array, but slightly increases as the optimal size of the BTES increases with the CO_2 price, as it can be seen in Fig. 10. This is lowering its operating temperature and increasing the fraction of heat that the BTES can cover.

Fig. 11 presents how the system heat balance varies as function of the CO_2 price. As expected, in the standard cooling demand scenario (Fig. 11a), the contribution of the solar system to the energy balance is similar in both CO_2 intensity profiles scenarios. As the limited available heat rejected from cooling operations is cannot support the heating demand, an increase in CO_2 cost naturally results in a larger fraction of heat covered by the solar array via the BTES or supplied directly.

In the case of the increased cooling demand scenario (Fig. 11b), the heat rejected from cooling operations does not act as a bottleneck in the instance of rejecting heat to cover a larger fraction of heating demand. In this case, as the CO_2 increases and the solar array becomes economically viable, the fraction of BTES charging with the chiller operation is reduced in favour of a larger portion covered by the solar array.

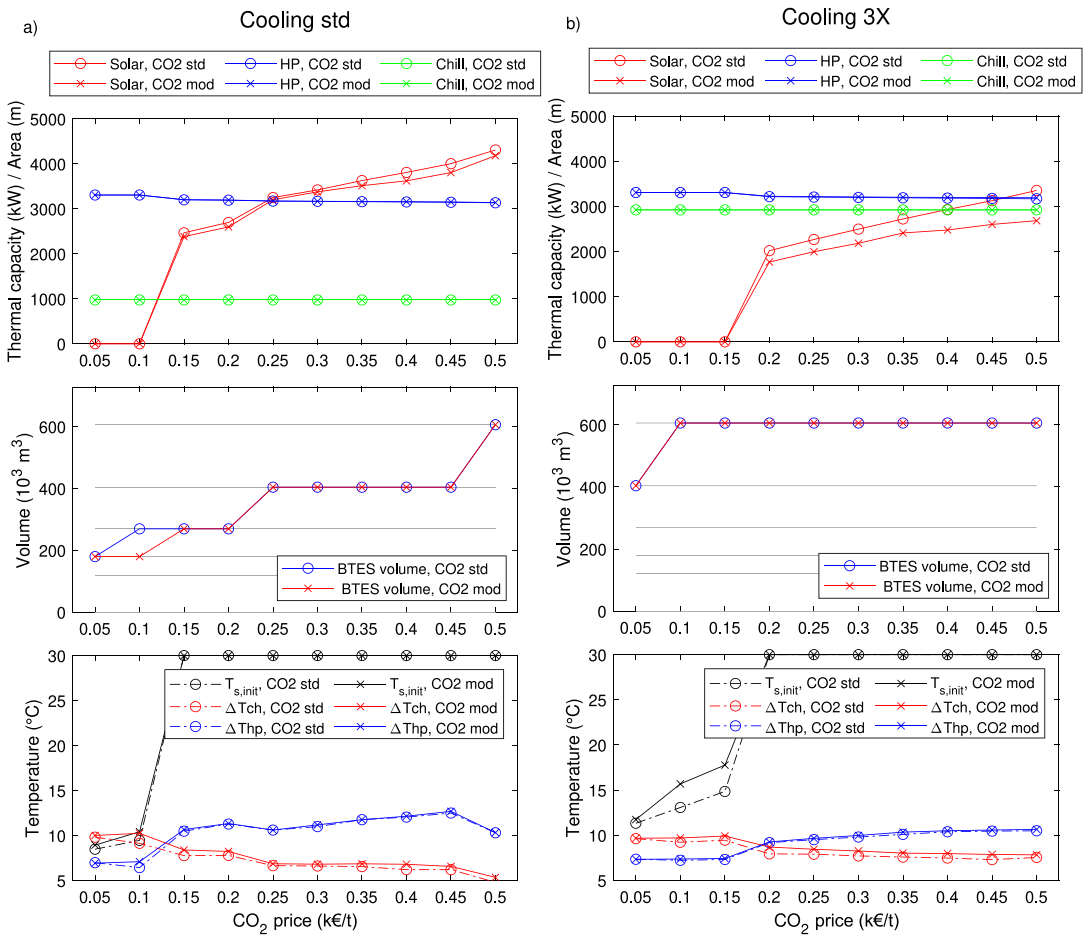

Fig. 8. Optimal solar, heat pump and chiller size (top), BTES size (top) and operation (bottom) as a function of the CO_2 price, in the (a) standard cooling demand and (b) increase cooling demand (3X) scenarios.

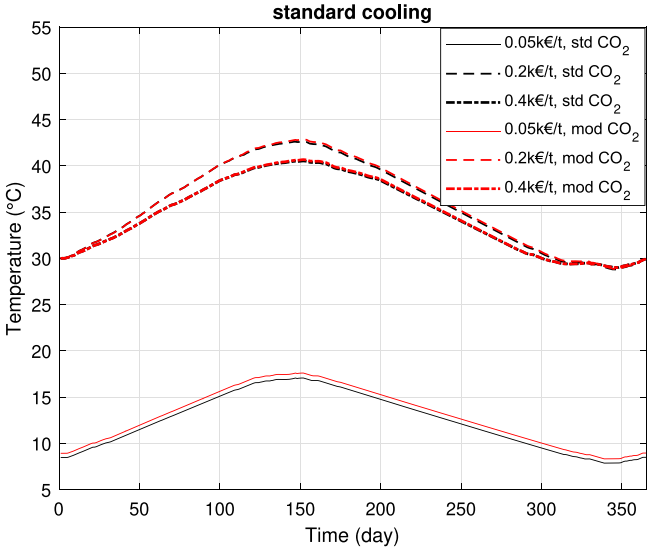

Fig. 9. Optimal temperature profile of the BTES in the standard cooling demand scenario, with the possibility of integrating solar generation, using different CO_2 prices and standard (std) and modified (mod) CO_2 intensity profiles.

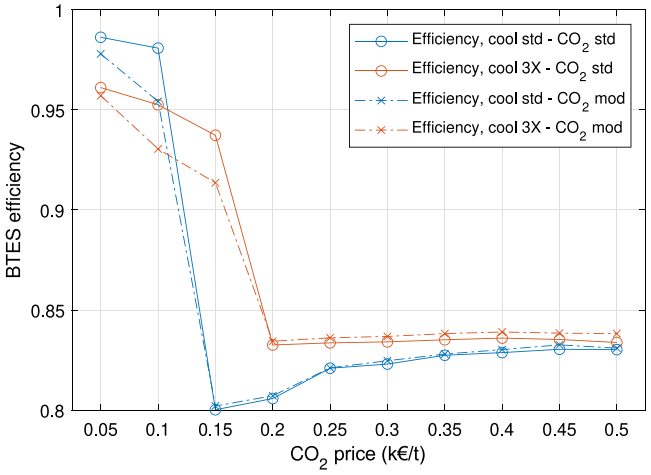

Fig. 10. Efficiency of the BTES in the various optimal system solutions found for different CO_2 costs, with the possibility of integrating solar generation.

This is an expected result, as the summer climate in the Zürich region is relatively mild, and exhausting the heat to the air is electricity-wise more efficient than charging a BTES operating at a higher temperature.

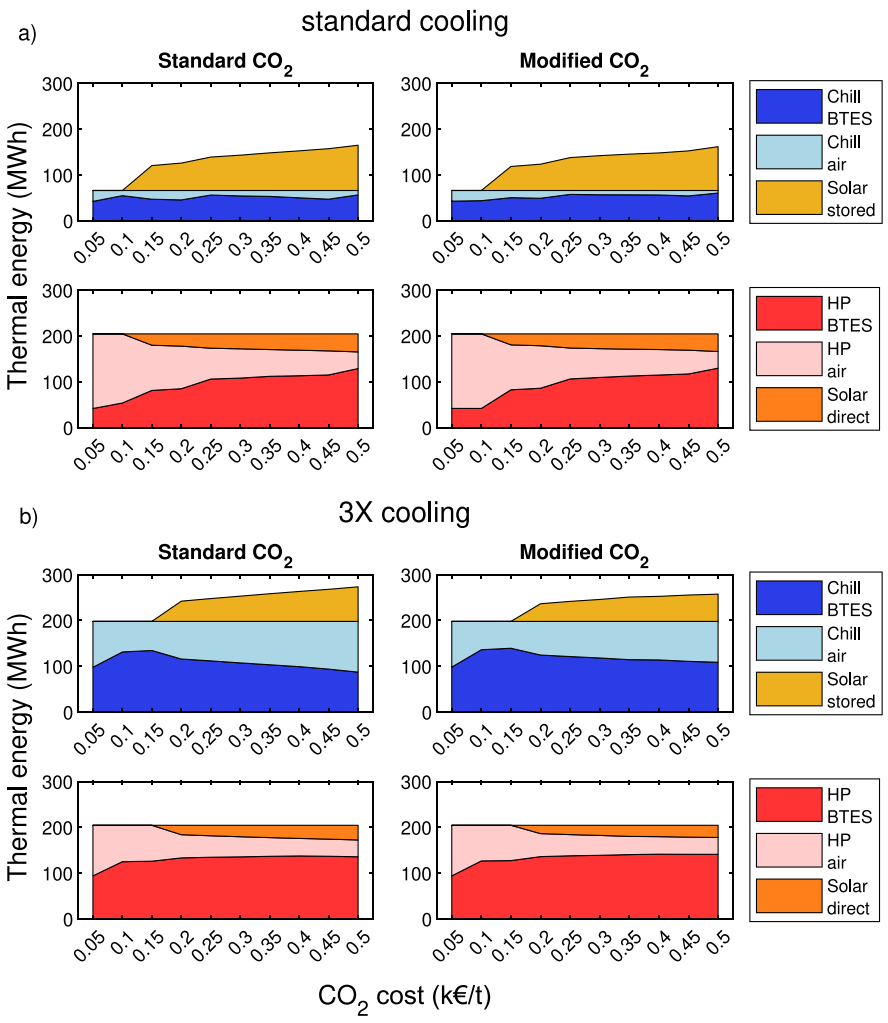

Fig. 11. Heating and cooling energy provided by the air-based or BTES-connected heat pump and chiller as function of the CO_2 cost and by the solar array (charging the BTES or directly to cover the heating demand), in (a) standard and (b) increased cooling (3X) scenarios.

As shown in Fig. 12, the possibility to include solar thermal generation enables a wider yearly CO_2 reduction range, even in the standard cooling demand scenarios. In the standard cooling scenario the reduction ranged from 3.9–4.1% with the lowest CO_2 price to 41.3–43.7% with the highest one. This was achieved with an annual cost ranging from 0.3% lower to 5.9–6.1% higher. In the increased cooling demand scenario the calculated reduction ranged from 9.0–9.7% with the lowest CO_2 price to 34.8–38.6% with the highest one, achieved with an annual cost ranging from 0.6% lower to 2.3–3.1% higher. As expected, the integration of a solar thermal array provides better system solutions at CO_2 prices higher than 0.10–0.15 k€/t, enabling a higher CO_2 reduction for the same annual cost as the case without solar.

5. Conclusions

This paper presented an optimization framework for the optimal design and operation of a district heating and cooling system integrating a borehole thermal energy storage BTES. In particular, differently from the optimization methods currently available in the literature, the proposed approach can take into consideration the combined effects of design and operation of such storage, such as the influence of the initial temperature of long-term storage temperature swing on the total capacity of the storage and thermal losses of the storage, the connection between the volume of the BTES storage and its maximum heat transfer rate, the effect of the temperature difference between the heat transfer fluid and storage on the heat transfer rate when the storage is charged

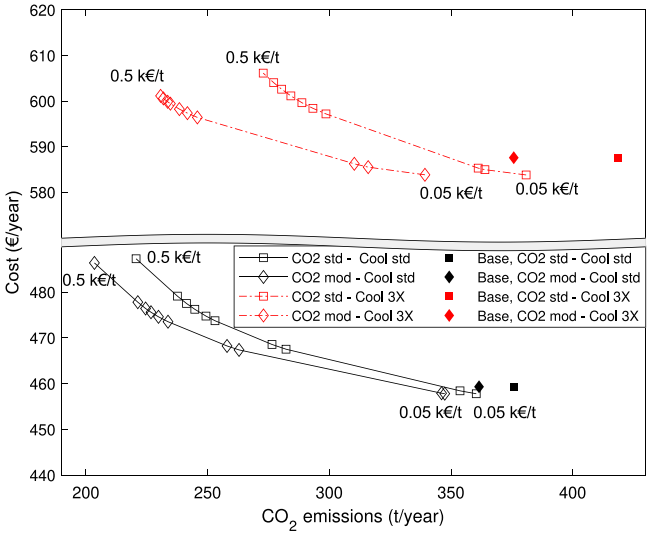

Fig. 12. Optimal system solutions under the different CO_2 intensity profile (square and rhomboidal markers) and cooling demand scenarios (black and red lines), with the integration of solar generation. The "base" setup, without a BTES or solar collectors, is presented with a filled marker for each scenario.

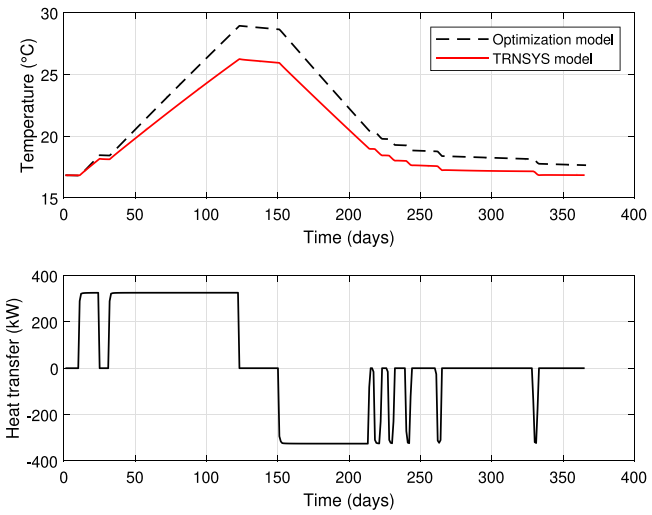

Fig. A.13. Comparison of the temperature response of the BTES model employed in the optimization against a detailed TRNSYS 18 (TRNSBM model) simulation, in the 7th year of operation for a BTES with diameter and depth equal to 51 m, imposing the same heat transfer profile. The model employed in the optimization slightly underestimates the losses, resulting in an end temperature 0.8 °C higher, and an efficiency of 83% compared to the 77% of TRNSYS.

or discharged and its implications on the COP of connected heat pumps or chillers. The proposed approach was applied to a heat pump and chiller-driven case study, based on the district heating and cooling demand of the Empa campus in Switzerland. To assess the impact of boundary conditions on the optimal design and operation of a BTES, two different cooling demand scenarios (one standard, with the cooling demand much lower than the heating one, and one where the cooling demand was increased to a level comparable to the heating one) and two electricity CO_2 intensity profiles (one standard, and with a summer intensity reduced by 2/3) were tested. The primary objective of the optimization was reducing the total system CO_2 emissions and its total cost. Varying prices associated with the carbon emissions were used to assign a higher or lower priority to the CO_2 emissions component. Results show that, when only considering the waste heat from cooling operations as a source of heat for the BTES, increasing the price of the CO_2 emissions would not only increase the optimal size of the BTES, but also its operating temperature, to take advantage of the seasonal variation in the CO_2 intensity profile. This was even more evident in the case of the modified CO_2 intensity profile, where this seasonal difference is enhanced, and in the case of increased cooling demand, where the limited rejected heat from cooling operations does not constitute a bottleneck in supporting the larger heating demand. When the possibility to integrate solar thermal collectors as an additional heat source was considered, the optimal size of the BTES increased with the CO_2 price also in this case, together with the size of the solar array as soon as the integration of solar collectors became economically viable (above a CO_2 price of 0.1–0.15 k€/t). At the same time, the optimal operation of the BTES changed, working at a higher temperature as soon as the solar generation was introduced in the system design. The optimal size of the solar collector array was influenced by the cooling demand (a smaller cooling demand resulted in larger collector areas, to compensate for the lower amount of rejected heat) as well as the CO_2 intensity profile (a larger intensity seasonal difference lead to smaller collector areas, as it is more beneficial to use even less efficient cooling operations to charge the BTES).

While the opportunity of reducing the CO_2 emissions, compared to a baseline system without a BTES, was quite limited in the case of a system without solar collectors and with standard cooling demand and CO_2 intensity profile (from 4.1 with the lowest CO_2 cost, up to 6.7% with the highest), an increase in cooling demand and modification of the CO_2 profile would improve the potential reduction up to 27.1%.

Including the possibility to integrate a solar thermal array enables the system design to further expand the potential CO_2 emissions reduction, to a range of 3.9–9.7% with the lowest CO_2 cost to 34.8–43.7% with the highest one. The annual cost to achieve this reduction, compared to a system without a BTES and solar collectors, varied from 0.3–0.6% lower to 2.3–6.1% higher.

In summary, these results show that BTES systems have the potential to significantly reduce CO_2 emissions of heat pump and chiller-driven heating and cooling district heating systems, particularly when supported by additional renewable thermal energy sources to compensate for missing energy to cover heating demand. The BTES operational conditions are also critical in ensuring the system is sized correctly, as the best solution was found to vary, depending on the boundary conditions, from a low-temperature storage, operating around the undisturbed ground temperature to maximize energy efficiency, to a high-temperature storage that could enhance the benefits of increasing the efficiency of the heat extraction in wintertime. As an outlook for future work, benchmarking of different optimal design methods, implementing the obtained solutions in a high detail modelling platform and verify their optimality in a realistic setting is considered a natural valuable continuation of this research stream.

CRediT authorship contribution statement

Massimo Fiorentini: Conceptualization, Methodology, Investigation, Formal analysis, Writing – original draft. **Philipp Heer:** Writing – review & editing. **Luca Baldini:** Conceptualization, Methodology, Writing – review & editing.

Declaration of competing interest

The authors declare that they have no known competing financial interests or personal relationships that could have appeared to influence the work reported in this paper.

Data availability

Data will be made available on request.

Acknowledgements

The authors thank K. Orehounig for her insights on the energy hub approach and relevant applications to seasonal thermal energy storage, and acknowledge the financial support of the Swiss Federal Office of Energy SFOE grant No. SI/501938.

Appendix

In this section additional results are provided in support of the discussion of the paper. The comparison in Fig. A.13, where the optimization model and the TRNSYS (TRNSBM) model are subject to the same heat transfer profile, gives an indication of the mismatch between the more detailed and the optimization-oriented model.

Fig. A.14 provides a summary of the overall system performance in heating and cooling when the different optimal design solutions, as a function of the CO_2 price, CO_2 intensity profile and cooling profile, are employed. Fig. A.15 shows in more detail the individual COP distribution of the air- and BTES-source heat pumps and chiller in two different CO_2 price scenarios, under the same CO_2 intensity and cooling profile conditions.

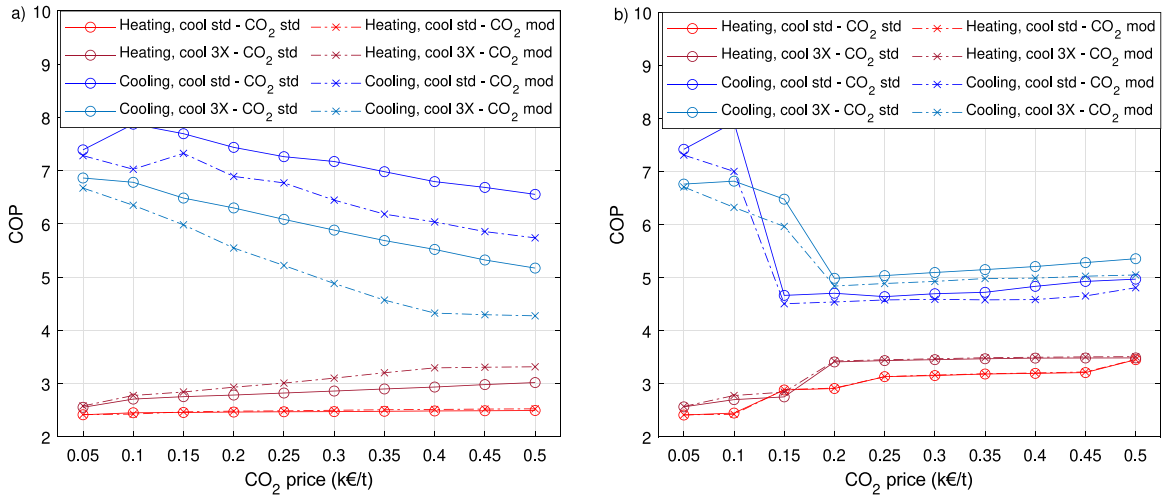

Fig. A.14. Average system COP in cooling and heating (including both air- and BTES-source heat pumps and chillers), as the system design and operation changes under the different CO_2 pricing scenarios. (a) results without solar thermal generation and (b) results with solar thermal generation.

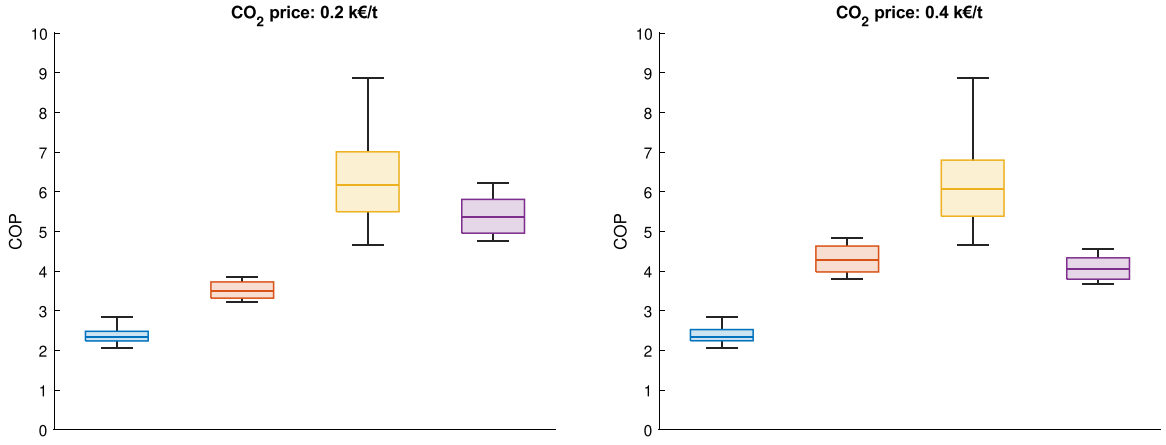

Fig. A.15. Example of COP distribution for the air-source and BTES-source heat pump and chiller in the scenario with modified CO_2 intensity profile and cooling 3X under the 0.2 k€/t CO_2 price condition (left) and 0.4 k€/t CO_2 price condition (right). A higher CO_2 price leads to a higher BTES temperature, and consequently a lower BTES chiller COP, but higher BTES heat pump COP.

References

[1] International Energy Agency. Renewables 2020. Tech. rep., 2020, URL https://www.iea.org/reports/renewables-2020.

[2] Dahash A, Ochs F, Janetti MB, Streicher W. Advances in seasonal thermal energy storage for solar district heating applications: A critical review on large-scale hot-water tank and pit thermal energy storage systems. Appl Energy 2019;239:296–315. http://dx.doi.org/10.1016/j.apenergy.2019.01.189, URL http://www.sciencedirect.com/science/article/pii/S0306261919301837.

[3] Mangold D, Deschaintre L. Seasonal thermal energy storage - Report on state of the art and necessary further R + D. In: IEA-SHC Task 45 large systems. 2015, p. 1–48, URL http://task45.iea-shc.org/data/sites/1/publications/IEA_SHC_Task45_B_Report.pdf.

[4] Rosato A, Ciervo A, Ciampi G, Scorpio M, Sibilio S. Impact of seasonal thermal energy storage design on the dynamic performance of a solar heating system serving a small-scale Italian district composed of residential and school buildings. J Energy Storage 2019;25:100889. http://dx.doi.org/10.1016/J.EST.2019.100889.

[5] Elhashmi R, Hallinan KP, Chiasson AD. Low-energy opportunity for multi-family residences: A review and simulation-based study of a solar borehole thermal energy storage system. Energy 2020;204:117870. http://dx.doi.org/10.1016/J.ENERGY.2020.117870.

[6] Sibbitt B, McClenahan D, Djebbar R, Thornton J, Wong B, Carriere J, et al. The performance of a high solar fraction seasonal storage district heating system – five years of operation. Energy Procedia 2012;30:856–65. http://dx.doi.org/10.1016/j.egypro.2012.11.097.

[7] Nußbicker-Lux J. The BTES project in Crailsheim (Germany) - Monitoring results. 2012.

[8] Buffa S, Cozzini M, D'Antoni M, Baratieri M, Fedrizzi R. 5Th generation district heating and cooling systems: A review of existing cases in Europe. Renew Sustain Energy Rev 2019;104:504–22. http://dx.doi.org/10.1016/j.rser.2018.12.059, URL http://www.sciencedirect.com/science/article/pii/S1364032118308608.

[9] Evins R. A review of computational optimisation methods applied to sustainable building design. Renew Sustain Energy Rev 2013;22:230–45. http://dx.doi.org/10.1016/J.RSER.2013.02.004, URL https://www.sciencedirect.com/science/article/pii/S1364032113000920.

[10] Sameti M, Haghighat F. Optimization approaches in district heating and cooling thermal network. In: Energy and Buildings. 140, Elsevier Ltd; 2017, p. 121–30. http://dx.doi.org/10.1016/j.enbuild.2017.01.062.

[11] Geidl M, Koeppel G, Favre-Perrod P, Klockl B, Andersson G, Frohlich K. Energy hubs for the future. IEEE Power Energy Mag 2007;5(1):24–30. http://dx.doi.org/10.1109/MPAE.2007.264850.

[12] Evins R, Orehounig K, Dorer V, Carmeliet J. New formulations of the 'energy hub' model to address operational constraints. Energy 2014;73:387–98. http://dx.doi.org/10.1016/J.ENERGY.2014.06.029, URL https://www.sciencedirect.com/science/article/pii/S0360544214007270.

[13] Baniasadi A, Habibi D, Al-Saedi W, Masoum MA, Das CK, Mousavi N. Optimal sizing design and operation of electrical and thermal energy storage systems in smart buildings. J Energy Storage 2020;28:101186. http://dx.doi.org/10.1016/J.EST.2019.101186, URL https://www.sciencedirect.com/science/article/pii/S2352152X19311545.

[14] Omu A, Hsieh S, Orehounig K. Mixed integer linear programming for the design of solar thermal energy systems with short-term storage. Appl Energy 2016;180:313–26. http://dx.doi.org/10.1016/j.apenergy.2016.07.055.

[15] Mehleri ED, Sarimveis H, Markatos NC, Papageorgiou LG. Optimal design and operation of distributed energy systems: Application to Greek residential sector.

Renew Energy 2013;51:331–42. http://dx.doi.org/10.1016/J.RENENE.2012.09.009.
[16] Harb H, Reinhardt J, Streblow R, Müller D. MIP approach for designing heating systems in residential buildings and neighbourhoods. J Build Perform Simul 2015;9(3):316–30. http://dx.doi.org/10.1080/19401493.2015.1051113.
[17] Klein S. TRNSYS, a transient system simulation program. Solar Energy Laboratory, University of Wisconsin–Madison; 1979.
[18] Shah SK, Aye L, Rismanchi B. Multi-objective optimisation of a seasonal solar thermal energy storage system for space heating in cold climate. Appl Energy 2020;268:115047. http://dx.doi.org/10.1016/j.apenergy.2020.115047.
[19] Tulus V, Boer D, Cabeza LF, Jiménez L, Guillén-Gosálbez G. Enhanced thermal energy supply via central solar heating plants with seasonal storage: A multi-objective optimization approach. Appl Energy 2016;181:549–61. http://dx.doi.org/10.1016/j.apenergy.2016.08.037.
[20] Antoniadis CN, Martinopoulos G. Optimization of a building integrated solar thermal system with seasonal storage using TRNSYS. Renew Energy 2019;137:56–66. http://dx.doi.org/10.1016/j.renene.2018.03.074.
[21] Prasanna A, Dorer V, Vetterli N. Optimisation of a district energy system with a low temperature network. Energy 2017;137:632–48. http://dx.doi.org/10.1016/j.energy.2017.03.137.
[22] Gabrielli P, Gazzani M, Martelli E, Mazzotti M. Optimal design of multi-energy systems with seasonal storage. Appl Energy 2018;219:408–24. http://dx.doi.org/10.1016/J.APENERGY.2017.07.142, URL https://www.sciencedirect.com/science/article/pii/S0306261917310139.
[23] Wirtz M, Kivilip L, Remmen P, Müller D. 5Th Generation District Heating: A novel design approach based on mathematical optimization. Appl Energy 2020;260:114158. http://dx.doi.org/10.1016/j.apenergy.2019.114158.
[24] Miglani S, Orehounig K, Carmeliet J. Integrating a thermal model of ground source heat pumps and solar regeneration within building energy system optimization. Appl Energy 2018;218:78–94. http://dx.doi.org/10.1016/J.APENERGY.2018.02.173.
[25] Steen D, Stadler M, Cardoso G, Groissböck M, DeForest N, Marnay C. Modeling of thermal storage systems in MILP distributed energy resource models. Appl Energy 2015;137:782–92. http://dx.doi.org/10.1016/j.apenergy.2014.07.036.
[26] Bischi A, Taccari L, Martelli E, Amaldi E, Manzolini G, Silva P, et al. A detailed MILP optimization model for combined cooling, heat and power system operation planning. Energy 2014;74:12–26. http://dx.doi.org/10.1016/J.ENERGY.2014.02.042, URL https://www.sciencedirect.com/science/article/pii/S0360544214001765.
[27] Mehrjerdi H, Rakhshani E. Optimal operation of hybrid electrical and thermal energy storage systems under uncertain loading condition. Appl Therm Eng 2019;160:114094. http://dx.doi.org/10.1016/J.APPLTHERMALENG.2019.114094, URL https://www.sciencedirect.com/science/article/pii/S1359431119313638.
[28] Wirtz M, Neumaier L, Remmen P, Müller D. Temperature control in 5th generation district heating and cooling networks: An MILP-based operation optimization. Appl Energy 2021;288:116608. http://dx.doi.org/10.1016/j.apenergy.2021.116608, URL https://linkinghub.elsevier.com/retrieve/pii/S0306261921001422.
[29] Leśko M, Bujalski W, Futyma K. Operational optimization in district heating systems with the use of thermal energy storage. Energy 2018;165:902–15. http://dx.doi.org/10.1016/j.energy.2018.09.141.
[30] Xu Q, Dubljevic S. Model predictive control of solar thermal system with borehole seasonal storage. Comput Chem Eng 2017;101:59–72. http://dx.doi.org/10.1016/j.compchemeng.2017.02.023, URL http://www.sciencedirect.com/science/article/pii/S009813541730087X.
[31] Gabrielli P, Acquilino A, Siri S, Bracco S, Sansavini G, Mazzotti M. Optimization of low-carbon multi-energy systems with seasonal geothermal energy storage: The Anergy Grid of ETH Zurich. Energy Convers Manag: X 2020;8(July):100052. http://dx.doi.org/10.1016/j.ecmx.2020.100052.
[32] Majewski DE, Wirtz M, Lampe M, Bardow A. Robust multi-objective optimization for sustainable design of distributed energy supply systems. Comput Chem Eng 2017;102:26–39. http://dx.doi.org/10.1016/j.compchemeng.2016.11.038.
[33] Petkov I, Gabrielli P. Power-to-hydrogen as seasonal energy storage: an uncertainty analysis for optimal design of low-carbon multi-energy systems. Appl Energy 2020;274:115197. http://dx.doi.org/10.1016/j.apenergy.2020.115197.
[34] Yokoyama R, Shinano Y, Taniguchi S, Ohkura M, Wakui T. Optimization of energy supply systems by MILP branch and bound method in consideration of hierarchical relationship between design and operation. Energy Convers Manage 2015;92:92–104. http://dx.doi.org/10.1016/J.ENCONMAN.2014.12.020, URL https://www.sciencedirect.com/science/article/pii/S0196890414010498.
[35] Hellström G. Ground heat storage: Thermal analyses of duct storage systems. Lund University; 1991, p. 310, URL http://search.proquest.com/docview/303983441?accountid=14357, ISBN 91-628-0290-9.
[36] Pahud D, Fromentin A, Hadorn JC. The superposition borehole model for TRNSYS (TRNSBM). Tech. rep., User Manuel, Internal Report, LASEN-EPFL, Lausanne; 1996.
[37] Fiorentini M, Baldini L. Control-oriented modelling and operational optimization of a borehole thermal energy storage. Appl Therm Eng 2021;117518. http://dx.doi.org/10.1016/J.APPLTHERMALENG.2021.117518, URL https://linkinghub.elsevier.com/retrieve/pii/S1359431121009492.
[38] Gurobi. Gurobi Solver. URL https://www.gurobi.com/products/gurobi-optimizer/.
[39] Lawrie L, Drury C. Development of global typical meteorological years (TMYx). 2019, URL http://climate.onebuilding.org.
[40] electricitymap. URL https://www.electricitymap.org/map.
[41] Weber R, Baldini L. High temperature seasonal BTES for effective load shifting and CO2 emission reduction. In: Eurosun 2018 – 12th international conference on solar energy for buildings and industry. (September):Rapperswil, Switzerland; 2018, p. 1–9. http://dx.doi.org/10.18086/eurosun2018.13.04.
[42] Luo J, Rohn J, Bayer M, Priess A. Thermal performance and economic evaluation of double U-tube borehole heat exchanger with three different borehole diameters. Energy Build 2013;67:217–24. http://dx.doi.org/10.1016/j.enbuild.2013.08.030.
[43] Skarphagen H, Banks D, Frengstad BrS, Gether H. Design considerations for borehole thermal energy storage (BTES): A review with emphasis on convective heat transfer. Geofluids 2019;2019. http://dx.doi.org/10.1155/2019/4961781.
[44] ElCom electricity tariffs. URL https://www.strompreis.elcom.admin.ch.
[45] EMBER Daily EU ETS carbon price. URL https://ember-climate.org/data/carbon-price-viewer/.
[46] IEA. Levelised cost of CO2 capture by sector and initial CO2 concentration. 2019, URL https://www.iea.org/data-and-statistics/charts/levelised-cost-of-co2-capture-by-sector-and-initial-co2-concentration-2019.
[47] Löfberg J. YALMIP : A toolbox for modeling and optimization in MATLAB. In: In proceedings of the CACSD conference. Taipei, Taiwan; 2004.